Joule

CellPress

Article

An Unlikely Route to Low Lattice Thermal Conductivity: Small Atoms in a Simple Layered Structure

Wanyue Peng, Guido Petretto, Gian-Marco Rignanese, Geoffroy Hautier, Alexandra Zevalkink

geoffroy.hautier@uclouvain.be (G.H.)
alexzev@msu.edu (A.Z.)

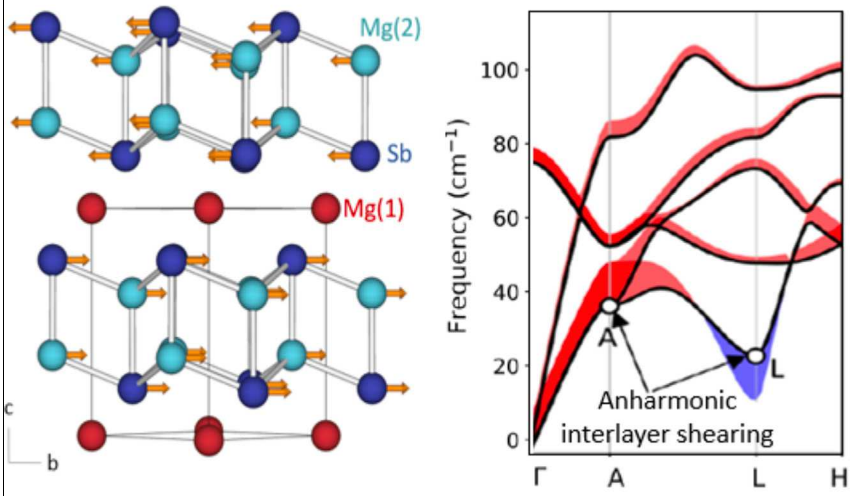

The layered compound Mg_3Sb_2 exhibits low lattice thermal conductivity despite its low density and simple structure. To explain the anomalous thermal behavior of Mg_3Sb_2, we explore trends in the elasticity, thermal expansion, and anharmonicity of AMg_2Pn_2 Zintl compounds with A = Mg, Ca, and Yb, and Pn = Sb and Bi. Phonon calculations and high-temperature speed-of-sound measurements reveal large mode Grüneisen parameters in Mg_3Sb_2 compared with isostructural compounds, in particular in transverse acoustic modes involving shearing of adjacent layers.

HIGHLIGHTS

Mg_3Sb_2 shows anomalous thermal behavior relative to isostructural compounds

Low thermal conductivity in Mg_3Sb_2 is due to highly anharmonic shear modes

Undersized cations may lead to low thermal conductivity in ionic compounds

Peng et al., Joule *2*, 1–15
October 17, 2018 © 2018 Elsevier Inc.
https://doi.org/10.1016/j.joule.2018.06.014

Please cite this article in press as: Peng et al., An Unlikely Route to Low Lattice Thermal Conductivity: Small Atoms in a Simple Layered Structure, Joule (2018), https://doi.org/10.1016/j.joule.2018.06.014

Joule

CellPress

Article

An Unlikely Route to Low Lattice Thermal Conductivity: Small Atoms in a Simple Layered Structure

Wanyue Peng,[1] Guido Petretto,[2] Gian-Marco Rignanese,[2] Geoffroy Hautier,[2,*] and Alexandra Zevalkink[1,3,*]

SUMMARY

The layered compound Mg_3Sb_2 exhibits low lattice thermal conductivity comparable with PbTe and Bi_2Te_3, despite its low density and simple structure. To explain the origins of the low thermal conductivity in Mg_3Sb_2, we use experimental and theoretical methods to explore trends in the elasticity, thermal expansion, and anharmonicity of AMg_2Pn_2 Zintl compounds with A = Mg, Ca, and Yb, and Pn = Sb and Bi. Phonon calculations reveal large mode Grüneisen parameters in Mg_3Sb_2 compared with isostructural compounds, in particular in transverse acoustic modes involving shearing of adjacent layers. High-temperature resonant ultrasound spectroscopy confirms the rapid softening of the acoustic branches in Mg_3Sb_2. We attribute the anomalous thermal behavior of Mg_3Sb_2 to the diminutive size of Mg, which is too small for the octahedrally coordinated site, leading to weak interlayer bonding. These results suggest that undersized cations may provide a route to low lattice thermal conductivity, even in earth-abundant, low-density materials.

INTRODUCTION

The ability to predict and design thermal transport in bulk materials is a fundamental requirement for a wide range of energy applications.[1] In areas such as the development of thermal barrier coatings and thermoelectric devices, engineering materials with extremely low lattice thermal conductivity, κ_L, is vital. In materials with inherently high thermal conductivity (e.g., Si), low κ_L can be achieved using clever microstructural design, nanostructuring, point defects, or all of the above to scatter phonons.[2–5] Alternatively, inherently low κ_L can be achieved in compounds with low phonon velocities or high rates of phonon-phonon scattering. In the search for materials with low κ_L, compounds with high density (e.g., PbTe), soft bonds (e.g., Bi_2Te_3), and complex atomic structures (e.g., $Yb_{14}MnSb_{11}$[6]) are thus favored, since these features lead to low phonon velocities.[7] Design parameters for achieving high rates of phonon-phonon scattering (i.e., materials with large Grüneisen parameters, γ) are more elusive, although a number of studies have recently provided guidance here as well. For example, highly anharmonic phonon modes arise from soft or unstable bonds (e.g., associated with lone pairs, rattlers in cage compounds, resonance bonding[8–12]) and they generally emerge in the vicinity of lattice instabilities.[13,14]

The binary compound, Mg_3Sb_2, which crystallizes in the $CaAl_2Si_2$ structure type (Figure 1), appears to defy standard paradigms used to identify materials with low lattice thermal conductivity. Mg_3Sb_2 has a low density, relatively high speed of sound, and a simple atomic structure with only five atoms per primitive cell. Yet despite having

Context & Scale

In the search for materials with low lattice thermal conductivity, we typically look to compounds with high density, low speed of sound, and complexity at either the atomic or nano level. The layered compound Mg_3Sb_2 defies these paradigms, exhibiting low lattice thermal conductivity comparable with PbTe and Bi_2Te_3, despite its low density and simple atomic structure. While n-type Mg_3Sb_2 is an excellent thermoelectric material ($zT > 1.6$), its thermal properties remain largely unstudied. In the present study, we probe the origins of low lattice thermal conductivity of Mg_3Sb_2 by exploring the lattice dynamics of a series of isostructural compounds in the $CaAl_2Si_2$ structure type. Although the ionic interlayer bonds in this structure type are usually strong, we find that undersized cations can lead to soft and highly anharmonic transverse phonons. These results point to a potential route to achieving low lattice thermal conductivity in other layered compounds with ionic interlayer bonding.

Please cite this article in press as: Peng et al., An Unlikely Route to Low Lattice Thermal Conductivity: Small Atoms in a Simple Layered Structure, Joule (2018), https://doi.org/10.1016/j.joule.2018.06.014

roughly half the density of PbTe and Bi_2Te_3, it has comparable κ_L at room temperature (1–1.5 W/mK[15–17]). AM_2X_2 compounds with the $CaAl_2Si_2$ structure have attracted a great deal of interest for thermoelectric applications owing to their chemical diversity and flexibility in tuning transport properties.[18,19] However, compounds in this simple, layered Zintl structure type typically do *not* have low thermal conductivity, in part because the strong ionic bonds between the covalent M_2X_2 slabs lead to high overall bond stiffness, especially compared with traditional layered compounds containing van der Waals bonds. As illustrated by Figure 2A, the low κ_L of Mg_3Sb_2 is anomalous compared with other AM_2X_2 compounds with the $CaAl_2Si_2$ structure type. Although Mg_3Sb_2 is one of the lightest compounds in the series, it exhibits one of the lowest values of κ_L. In particular, we note that the reported κ_L of Mg_3Sb_2 is three times lower than that of $CaMg_2Sb_2$,[20] which differs only by the presence of Ca instead of Mg on the octahedral site.

Recently, excellent thermoelectric performance was demonstrated in *n*-type $Mg_3(Sb,Bi)_2$ alloys, with zT up to 1.6 reported by several independent groups.[24–28] This surpasses all previous results for isostructural compounds, which have been exclusively *p*-type. To date, experimental and theoretical investigations of Mg_3Sb_2 have focused on the electronic properties; for example, the defect origin of *n*-type doping,[24,29] the multi-valley character of the conduction band,[25,27,30,31] and routes to increased carrier mobility.[28,32] In contrast, the anomalously low κ_L of both *n*- and *p*-type Mg_3Sb_2 has not been investigated, although it plays an equally important role in leading to the high zT. The aim of the present study is to shed light on the origins of low lattice thermal conductivity in Mg_3Sb_2. We employ experimental methods and *ab initio* phonon calculations to investigate trends in the thermal properties of binary and ternary AMg_2Pn_2 compounds with A = Mg, Ca, and Yb, and Pn = As, Sb, and Bi, revealing previously unrecognized soft shearing modes and highly anharmonic acoustic phonons in Mg_3Sb_2 and Mg_3Bi_2. This work shows that soft shear modes resulting from undersized cations provide a potential route to achieving low lattice thermal conductivity even in simple, low-density structures.

RESULTS AND DISCUSSION

Anomalously Low Lattice Thermal Conductivity in Mg_3Sb_2

Inherently low lattice thermal conductivity, κ_L, stems from either slow phonon velocities, v, or short phonon relaxation times, τ.[7,33] Of these two factors, the phonon velocities are the more accessible quantity; they can either be estimated roughly using the speed of sound, or can be obtained from the calculated or measured phonon dispersion. Thus, in investigating the origin of low κ_L in any material, we should always begin by asking whether or not low phonon velocity is responsible. In Figure 2B, we have plotted the experimental κ_L of AM_2X_2 compounds as a function of the predicted mean speed of sound, ν_s. We have only included data from unalloyed samples, most of which exhibit the $1/T$ temperature dependence expected for Umklapp scattering dominated transport. Due to the lack of experimental speed of sound data in most of the compounds, we used the calculated bulk and shear elastic moduli from Materials Project to estimate ν_s[22] (details can be found in Supplemental Information). A comparison of the experimental and computed speed of sound in the compounds in this study shows less than 7% difference, showing the reliability of this approach.

When thermal transport is limited by Umklapp phonon-phonon scattering, κ_L can be approximated as proportional to ν_s^3 (see the dashed curve in Figure 2B), assuming that the Grüneisen parameter, γ, remains constant for this structure

[1]Michigan State University, East Lansing, MI, USA

[2]Université catholique de Louvain, Louvain-la-Neuve, Belgium

[3]Lead Contact

*Correspondence:
geoffroy.hautier@uclouvain.be (G.H.),
alexzev@msu.edu (A.Z.)

https://doi.org/10.1016/j.joule.2018.06.014

Please cite this article in press as: Peng et al., An Unlikely Route to Low Lattice Thermal Conductivity: Small Atoms in a Simple Layered Structure, Joule (2018), https://doi.org/10.1016/j.joule.2018.06.014

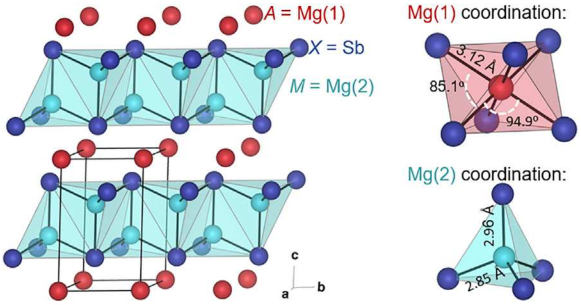

Figure 1. CaAl2Si2 Structure Type

Mg_3Sb_2 (alternatively written $MgMg_2Sb_2$) crystallizes in the $CaAl_2Si_2$ structure (space group $P\overline{3}m1$), characterized by anionic M_2X_2 slabs separated by A cations. In Mg_3Sb_2 and Mg_3Bi_2, the Mg(1) occupies the highly distorted octahedrally coordinated A site and Mg(2) the tetrahedrally coordinated M site.[21] The Mg-Sb bond lengths differ significantly in the two sites.

type.[7,33,34] This is not an unreasonable starting assumption, given that Grüneisen parameters can be correlated empirically with the average coordination number of a compound, which remains constant here.[35] Regardless, the data for AM_2X_2 compounds exhibit a great deal of spread, and clearly is not well described by this simple model. Much of the spread arises from differences in sample microstructure (note, for example, the variation in κ_L of nominally pure $YbZn_2Sb_2$ samples), but differences in the Grüneisen parameter also play an important role, as we discuss further below.

Despite the overall spread in the literature κ_L data, the binary compound Mg_3Sb_2 stands out as having particularly low κ_L. This implies either (a) that additional scattering sources are present and unique to Mg_3Sb_2 samples, (b) that the Grüneisen parameter of Mg_3Sb_2 is abnormally large, leading to increased Umklapp scattering, or (c) that the sound velocity fails to capture broader trends in the phonon group velocities in this structure type. We note that there is currently no evidence that the microstructure or defect concentrations in Mg_3Sb_2 samples differ strongly from other AM_2X_2 samples. Similar values for κ_L reported from multiple research groups and processing approaches lead us to believe that low κ_L is an inherent characteristic of Mg_3Sb_2.[15–17,26,28,29] Thus, in the current study we investigate the latter two possible explanations for low κ_L.

Ab Initio Phonon Calculations

To date, the calculated phonon density of states (DOS) and dispersion relations have only been reported for a small handful of compounds with the $CaAl_2Si_2$ structure type.[36,37] The atom-projected DOS shown for Mg_3Sb_2, $CaMg_2Sb_2$, and $CaMg_2Bi_2$ in Figure 3, are consistent with previous reports, which show sharply segmented frequency regimes. The anion displacement (Pn = Sb or Bi) dominates at low frequencies, cation displacement is responsible for the mid-frequency modes, and the M = Mg(2) site dominates the highest frequency range. In the case of Mg_3Sb_2, the partitioning of the two Mg sites reflects very significant differences in local bonding environment. From the lower phonon frequencies of the octahedrally coordinated Mg(1), we can infer that the Mg(1)-Sb bonds are much softer than the Mg(2)-Sb bonds. We note that the average phonon group velocities at high frequencies in Mg_3Sb_2 do not appear to be significantly different from $CaMg_2Sb_2$. We can therefore rule out differences in the phonon group velocity as the primary origin of the low lattice thermal conductivity in Mg_3Sb_2.

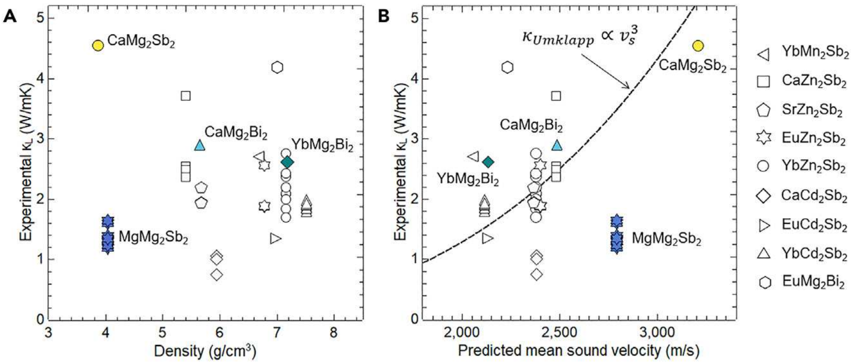

Figure 2. Comparison of Lattice Thermal Conductivity

(A and B) The experimental lattice thermal conductivity, κ_L, of Mg_3Sb_2 is significantly lower than isostructural AM_2X_2 compounds with similar (A) density and (B) predicted speed of sound (κ_L data can be found in Peng et al.[19]). The mean speed of sound, v_s, was estimated using the calculated elastic moduli from MaterialsProject.org and experimental densities.[22,23] The dashed line is shown as a guide to the eye representing the v_s dependence associated with Umklapp scattering, if all else remains constant.[7] Compounds shown in color are the primary focus of the current study.

Acoustic phonons tend to have an outsized influence on thermal transport due to the strong frequency dependence of Umklapp ($\tau \propto 1/\omega^2$) and point defect scattering ($\tau \propto 1/\omega^4$),[7,38] which leads to long mean free paths for these low-frequency phonons. The acoustic branches also tend to have higher group velocities than the optical branches, which further amplifies their relative contribution to κ_L. Any mechanism that preferentially slows or scatters acoustic phonons, therefore, can have an enormous impact on κ_L. Given that the acoustic phonons are dominated by displacement of the anions (Figure 3), it is perhaps surprising that the cation species (Mg or Ca) would greatly affect the phonon transport. The major differences between $CaMg_2Sb_2$ and Mg_3Sb_2 first become clear when we consider the phonon dispersion relations and their dependence on unit cell volume. The phonon dispersions are shown in Figure 4 in the low-frequency range only, as these show the greatest change with respect to composition (the full dispersions are shown in Figure S2). The magnitude and sign of the mode Grüneisen parameters, γ_i, are represented by the thickness and color of the dispersion curves. Since the values are all scaled with a common factor, the curve thickness is representative of the relative values of the Grüneisen parameter.

We note that the predicted slope (i.e., phonon velocity) and volume dependence of the longitudinal acoustic branches are similar in $CaMg_2Sb_2$ and Mg_3Sb_2. In contrast, the transverse phonon modes are much softer (lower velocity) and have stronger volume dependence in Mg_3Sb_2. The mode Grüneisen parameters of the transverse phonons in Mg_3Sb_2 are particularly large at the Brillouin zone edge at the *A*, *L*, and *M* points. The modes with the largest magnitude of γ_i involve the shearing displacement of adjacent anionic slabs in the structure. This is illustrated in Figure 5, which shows snapshots of the displacement in the Mg_3Sb_2 structure for transverse acoustic phonons at the *A* point (largest positive γ_i) and at the *L* point (largest negative γ_i).

The mode-averaged Grüneisen parameters, γ, obtained from Equation 2 for Mg_3Sb_2, $CaMg_2Sb_2$, and $CaMg_2Bi_2$ are 1.83, 1.44, and 1.48, respectively. However, the averaged values fail to fully capture the contrast between Mg_3Sb_2 and the other two compounds. Figure 6 shows all of the mode Grüneisen parameters of Mg_3Sb_2

Please cite this article in press as: Peng et al., An Unlikely Route to Low Lattice Thermal Conductivity: Small Atoms in a Simple Layered Structure, Joule (2018), https://doi.org/10.1016/j.joule.2018.06.014

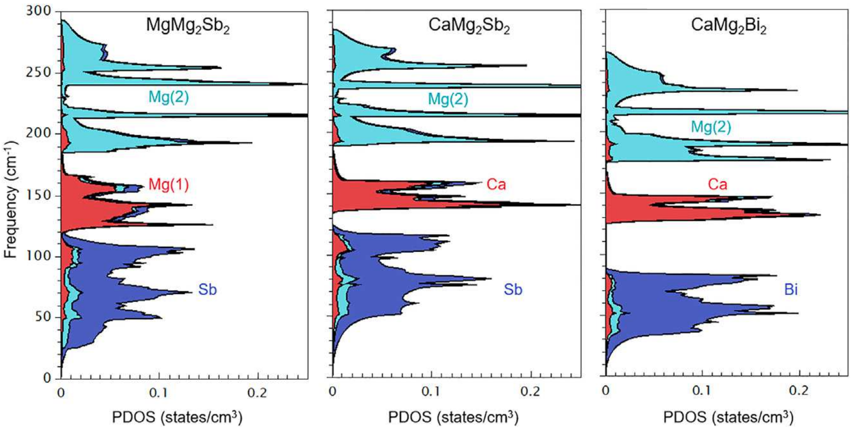

Figure 3. Phonon Density of States

The atom-projected phonon density of states of Mg_3Sb_2, $CaMg_2Sb_2$ and $CaMg_2Bi_2$ shows that the low-, mid-, and high-frequency regimes are dominated, respectively, by displacements of the anions (Sb, Bi), cations (Mg(1), Ca), and metal site (Mg(2)). The species on the cation site (Mg or Ca) does not strongly influence the maximum frequency or the average phonon velocities.

and $CaMg_2Sb_2$ as a function of frequency ($CaMg_2Bi_2$ is shown in the Figure S4). In the low-frequency acoustic regime, Mg_3Sb_2 has very large negative and positive γ_i values, both of which contribute strongly to phonon-phonon scattering. However, in the estimation of the mode-averaged γ, these contributions cancel each other out, thus obscuring the true impact. We note also that the values of γ_i in the optical frequency range from 120 to 150 cm^{-1} are much higher in Mg_3Sb_2 than in $CaMg_2Sb_2$. These phonon modes involve almost exclusively the displacement of the cation (Mg(1) or Ca), further indication of unstable Mg(1)-Sb interlayer bonding. A comparison of values of the average Grüneisen parameters and lattice thermal conductivity can be seen in Table S2. Animations of these phonon modes as well as an optical mode with Mg(1) motion can be found in Videos S1, S2, and S3.

Experimental Elastic Properties and Thermal Expansion

The speed of sound and the elastic moduli are determined solely by the slope of the acoustic branches of the phonon dispersion at the Γ point. Thus, measuring the high-temperature elasticity offers a window into the behavior of the acoustic phonons near the Γ point as a function of both temperature and unit cell volume, and can be used to evaluate the anharmonicity of these critical phonons. In the present study, resonant ultrasound spectroscopy (RUS) was used to obtain the elastic moduli, C11 and C44, of polycrystalline AMg_2Pn_2 samples (A = Mg, Ca, Yb, and Pn = Sb, Bi) as a function of temperature, from which we obtain the shear and bulk moduli (G and K, respectively) and the transverse and longitudinal speed of sound (v_T and v_L, respectively). The details of the equations applied are listed in Supplemental Information. This method provides an accurate and non-destructive approach that has been used to study high-temperature elastic behavior of various classes of materials.[39,40] Note that the elastic moduli and sound velocities obtained from polycrystalline samples represent an average over all crystallographic directions.

The elastic moduli of solids tend to become softer with increasing bond length.[34] Within compounds in the same structural pattern, if the unit cell volume increases, the elastic moduli are therefore expected to decrease. As shown in Figure 7, this trend is observed in AMg_2Pn_2 compounds in both the experimental (A = Mg, Ca, Yb and Pn = Sb, Bi) and computational elastic moduli (A = Mg, Ca, Sr, Ba and

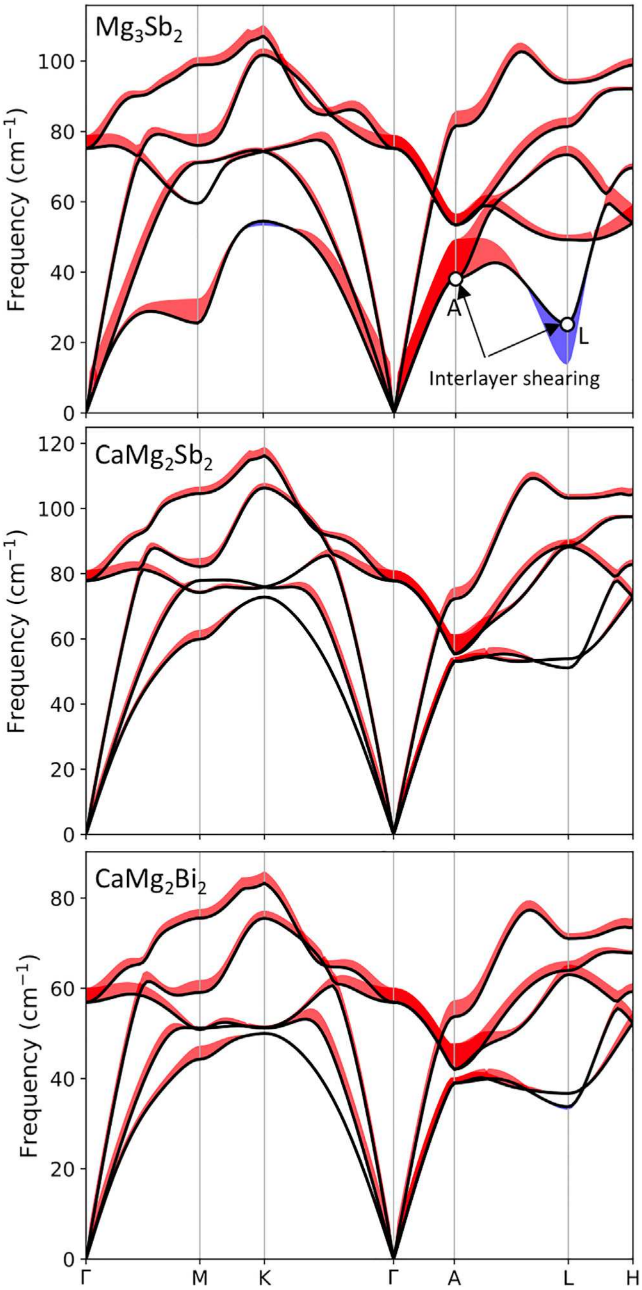

Figure 4. Phonon Dispersions

The phonon dispersions of Mg_3Sb_2, $CaMg_2Sb_2$, and $CaMg_2Bi_2$ in the low-frequency regime. The mode Grüneisen parameters, γ_i, are shown through the thickness of the bands, with red and blue representing positive and negative values of γ_i, respectively. The details of phonon dispersion at each temperature can be found in Figure S3.

Pn = P, As, Sb, Bi) obtained from the Materials Project.[23] Note that we omitted the computed elastic moduli of rare-earth-containing compounds due to poor agreement with the experiment. These values are included in Table S1, however. The only significant outliers in Figure 7 are the shear moduli of Mg_3Sb_2 and Mg_3Bi_2, which are much softer than compounds with similar unit cell volume. This suggests that the Mg(1)-Sb bonds connecting neighboring layers are quite weak compared

Please cite this article in press as: Peng et al., An Unlikely Route to Low Lattice Thermal Conductivity: Small Atoms in a Simple Layered Structure, Joule (2018), https://doi.org/10.1016/j.joule.2018.06.014

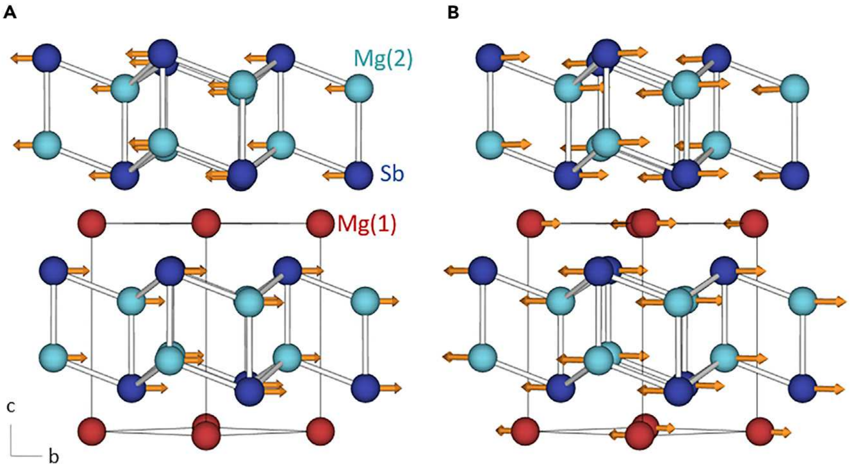

Figure 5. Atomic Displacement of Selected Phonon Modes
(A and B) Structure of Mg_3Sb_2 showing the atomic displacement corresponding to the transverse acoustic phonon modes (A) at the *A* point (large positive γ_i) and (B) at the *L* point (large negative γ_i). The corresponding modes are marked on the phonon dispersion in Figure 4.

with other AMg_2Pn_2 compounds. Soft shear moduli are often seen in layered compounds with weak van der Waals bonding[41–43] and, in the extreme case, disappearing shear modes at high temperature have been associated with liquid-like behavior.[44] In layered Zintl phases, however, the ionic bonds between adjacent anionic layers are expected to be strong, particularly in comparison with van der Waals solids. This is reflected by the relatively isotropic phonon dispersions of $CaMg_2Sb_2$ and $CaMg_2Bi_2$. The soft shear moduli in Mg_3Sb_2 and Mg_3Bi_2, in contrast, is anomalous. The weak bonding in Mg_3Sb_2 was reported in an earlier study of the elastic moduli of AM_2X_2 compounds,[45] but the impact on κ_L was not previously recognized.

Figures 8A and 8B show the experimental temperature dependence of the Young's and shear moduli of AMg_2Pn_2 samples with A = Mg, Ca, Yb and Pn = Sb, Bi. We have included the high-temperature Young's modulus of $Si_{0.8}Ge_{0.2}$,[39] PbTe[46], and SnTe[47] for comparison. In a purely harmonic model, the elastic moduli do not soften with increasing temperature. The degree to which a material deviates from this behavior can be used to quantify the degree of anharmonicity. $Si_{0.8}Ge_{0.2}$ softens slowly with respect to temperature, consistent with its small Grüneisen parameter (γ = 1.06 in pure Si[48]), while PbTe and SnTe, which are known to be highly anharmonic and soften more rapidly (γ = 2.1 in PbTe[46]). Over the measured temperature range, we find that the elastic moduli of Mg_3Bi_2 and Mg_3Sb_2 soften by ~25%, in comparison with only a ~5% decrease for $CaMg_2Pn_2$ and $YbMg_2Pn_2$ samples. The rate of softening of the elastic moduli with increasing temperature ($\partial G/\partial T$ and $\partial Y/\partial T$) is rapid in Mg_3Bi_2 and Mg_3Sb_2 even compared with PbTe and SnTe, providing direct evidence of the high anharmonicity in the acoustic branches of these compounds.

The thermal expansion coefficients (α) of the compounds in this study were measured using high-temperature X-ray diffraction (shown in Figure S1). For comparison, the computed thermal expansion and the temperature-dependent elastic moduli of Mg_3Sb_2, $CaMg_2Sb_2$, and $CaMg_2Bi_2$ are shown in Figures S5 and S6, respectively. Experimentally, we find that Mg_3Sb_2 and Mg_3Bi_2 have higher thermal expansion than other AMg_2Pn_2 (A = Ca, Yb and Pn = Sb, Bi) compounds, as expected given their higher Grüneisen parameters. However, the contrast between the

Please cite this article in press as: Peng et al., An Unlikely Route to Low Lattice Thermal Conductivity: Small Atoms in a Simple Layered Structure, Joule (2018), https://doi.org/10.1016/j.joule.2018.06.014

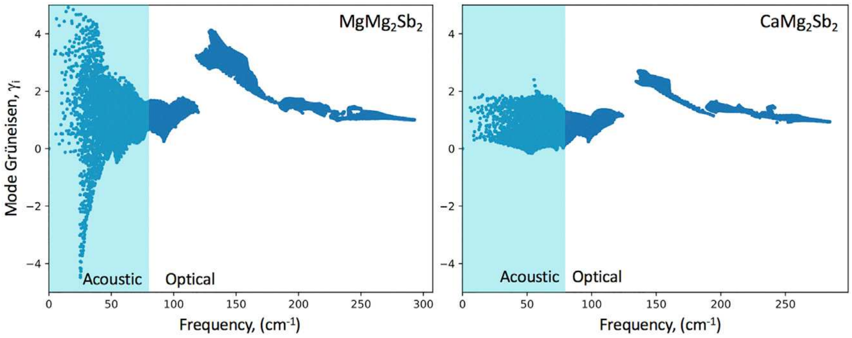

Figure 6. Mode Grüneisen Parameters

The mode Grüneisen parameters as a function of frequency highlight the impact that the cation site (Mg versus Ca) has on the low-frequency, acoustic phonons. In contrast, optical phonons are not strongly affected. Data for $CaMg_2Bi_2$, which behaves similarly to $CaMg_2Sb_2$, are provided in Supplemental Information.

measured values of α in the binary versus the ternary variants is much less impressive than the difference in the temperature dependence of their elastic moduli, $\partial G/\partial T$ and $\partial Y/\partial T$. This likely reflects the stronger dependence of the $\partial G/\partial T$ and $\partial Y/\partial T$ on the acoustic branches, which, as shown above, are more anharmonic than the optical branches. We thus regard the measurement of $\partial G/\partial T$ and $\partial Y/\partial T$ as an indicator of the "acoustic Grüneisen parameter."[49]

Breaking Pauling's Radius Ratio Rule

Among the AMg_2Pn_2 compounds considered in this study, the soft shear moduli and high anharmonicity appear to be unique to the binary compounds Mg_3Sb_2 and Mg_3Bi_2. This begs the question of what is special about the presence of Mg(1) on the octahedrally coordinated cation site. One immediately apparent factor is the size of Mg, which is smaller than any other cation that can occupy the octahedral site (e.g., Ca, Yb, Sr, Eu, and Ba). Several studies have investigated the effect of the cation size in AM_2X_2 compounds,[50,51] finding that the $ThCr_2Si_2$ structure type (in which the cation is 8-fold coordinated) is preferred over the $CaAl_2Si_2$ structure type in compounds with large cations such as Ba, K, and Rb. Here, we consider the opposite extreme: cations that are too small. In the sphere-packing model proposed by Pauling for ionic solids, the smallest stable cation to anion radius ratio for an octahedral coordination is given by $r_{\mathrm{cation}}:r_{\mathrm{anion}} = 0.414$.[52] Figure 9 shows the estimated $r_{\mathrm{cation}}:r_{\mathrm{anion}}$ for AMg_2Pn_2 compounds. We employed ionic radii for the cations assuming a valence of 2+ and a coordination number of 6 from Giacovazzo[53] and Shannon and Prewitt.[54] The anionic radii were estimated empirically by taking the average A-Pn bond length and subtracting the corresponding cation radii, yielding $r_P = 1.93$ Å, $r_{As} = 2.07$ Å, $r_{Sb} = 2.23$ Å, and $r_{Bi} = 2.29$ Å. Using this approach, compounds with A = Mg have $r_{\mathrm{cation}}:r_{\mathrm{anion}}$ below the stability limit, while compounds with larger cations are predicted to be stable in a 6-fold coordinated environment.

In addition to being the smallest available A-site cation for this structure type, Mg is also the most electronegative of the cations. On the one hand, this means that the use of the ionic radii for A may be an underestimate in the case of Mg. Furthermore, it is difficult to decouple the effects of the high electronegativity of Mg (and thus differences in the nature of the A-Pn bonds) from the packing effects associated with the radii. A comparison of the Born effective charges calculated for the Mg_3Sb_2, $CaMg_2Sb_2$, and $CaMg_2Bi_2$ (shown in Table S3) suggests that Mg(1)-Sb bonds are indeed more covalent than Ca-Sb bonds. An in-depth analysis of the bond polarity

Please cite this article in press as: Peng et al., An Unlikely Route to Low Lattice Thermal Conductivity: Small Atoms in a Simple Layered Structure, Joule (2018), https://doi.org/10.1016/j.joule.2018.06.014

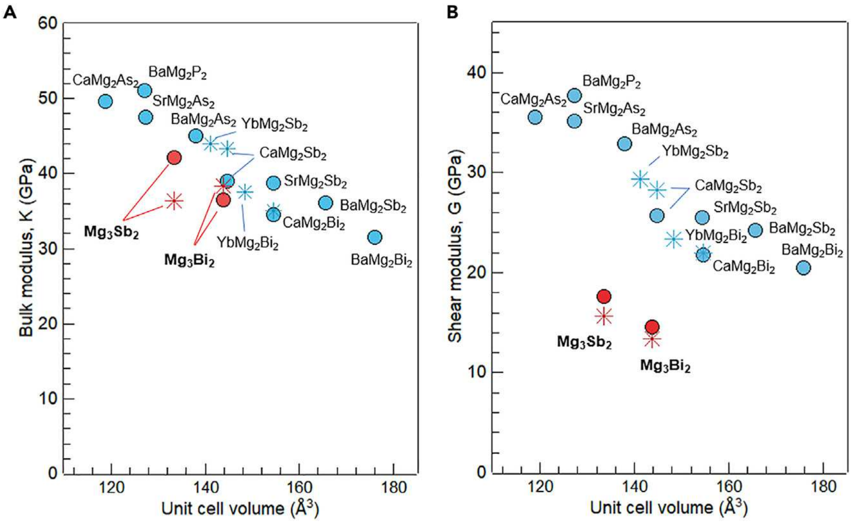

Figure 7. Comparison of Measured and Computed Elastic Moduli

(A and B) Experimental (asterisks) and computed (circles) elastic bulk (A) and shear (B) moduli of AMg_2Pn_2 compounds tend to decrease as a function of increasing unit cell volume and bond length. The anomalously low shear moduli of Mg_3Sb_2 and Mg_3Bi_2 are significant, suggesting soft bonding unique to these two binary compounds.[22]

in this structure type may be valuable in helping to explain the observed trends. If the Mg(1) effectively donates fewer than two valence electrons, its effective radius would also be larger, perhaps pushing the r_{cation}:r_{anion} ratio above the predicted stability limit.

There are additional factors, however, supporting the view that Mg is unstable in the octahedral site, including the strong distortion of the octahedral environment around Mg and the presence of a phase transition at high temperatures. The $MgPn_6$ octahedra in Mg_3Sb_2 and Mg_3Bi_2 exhibit bond angle variances of 26.53° and 36.01°, respectively. In comparison, the octahedral bond angle variance in $CaMg_2Sb_2$ and $CaMg_2Bi_2$ is only 1.77° and 5.04°. Furthermore, Mg_3Sb_2 and Mg_3Bi_2 are the only AMg_2Pn_2 compounds reported to undergo a structural phase transition at high temperature, which occurs at ~900°C and ~700°C, respectively.[55] In the cubic, high-temperature structure (Sc_2O_3 structure type, space group *Ia*3), Mg is tetrahedrally coordinated and satisfies Pauling's radius ratio rule.

The instability of the small Mg(1) cations in the octahedral *A* site of the $CaAl_2Si_2$ structure is likely responsible for both the unusually soft shear moduli and the highly anharmonic transverse phonon modes in Mg_3Sb_2 and Mg_3Bi_2. The weakening of ionic interlayer bonds would be expected to decrease the shear elastic moduli, and thus reduce the speed of sound relative to stiffer compounds (see Figure 8). As shown in Figure 2B, this effect alone is insufficient to explain the factor-of-three reduction in κ_L of Mg_3Sb_2 compared with $CaMg_2Sb_2$. It is likely that the undersized Mg(1) also has a destabilizing effect, leading to the observed high-temperature phase transition and also to the exceptionally high anharmonicity observed in modes associated with shearing of adjacent layers and motion of the Mg(1) cations (see Figures 4 and 5). "Giant anharmonicity" is well known to occur in the vicinity of lattice instabilities, as reported for PbTe, SnSe, and GeTe,[56,57] so it is not entirely surprising to see the same effect in this system as well. Above the phase transition

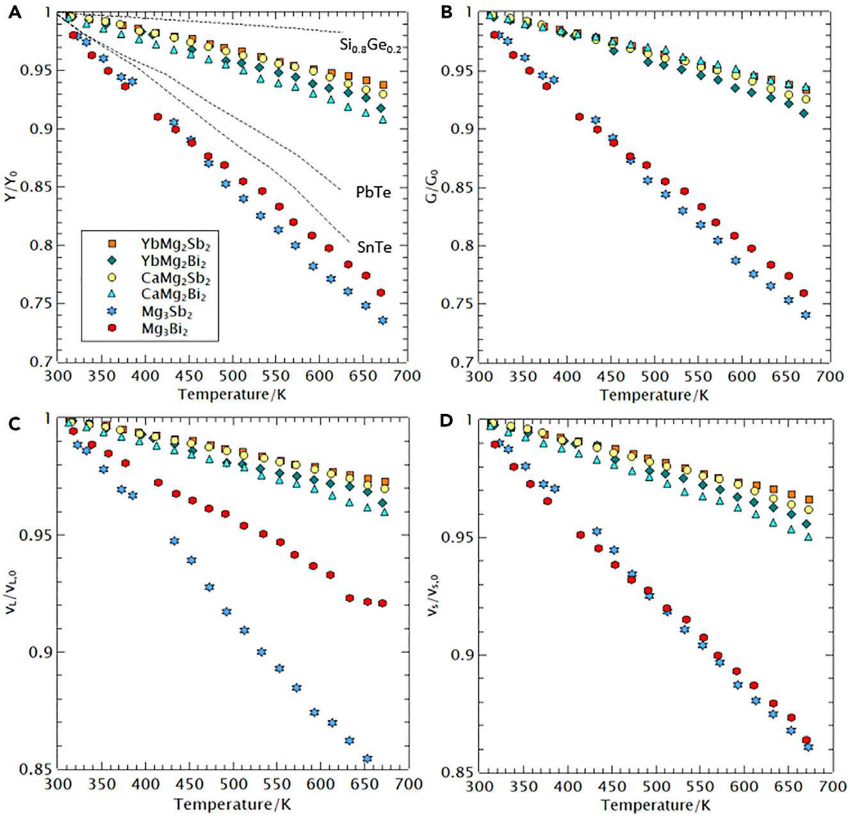

Figure 8. Temperature-Dependent Elastic Moduli

(A–D) Temperature-dependent (A) Young's modulus, (B) shear modulus, and (C) longitudinal and (D) transverse speed of sound measured using resonant ultrasound spectroscopy. Quantities were normalized to the room temperature value. Data for $Si_{0.8}Ge_{0.2}$, PbTe, and SnTe are from Li and Gladden,[39] Ren et al.,[46] and Schmidt et al.,[47] respectively.

in Mg_3Sb_2 and Mg_3Bi_2, we would expect the elastic moduli, speed of sound, and lattice thermal conductivity to exhibit a sharp increase.

Furthermore, the anharmonic behavior of Mg in Mg_3Sb_2 and Mg_3Bi_2 has parallels with the anharmonic rattling of Cu cations in $Cu_{12}Sb_4S_{13}$ tetrahedrite compounds[10] as well as with the under-coordinated *A*-site cations (i.e., too small) in perovskite compounds, which are known to lead to octahedral tilting and overall instability of the structure. The anharmonic Mg vibrational modes are also somewhat analogous to the rattling of filler atoms in their oversized cages in clathrates and skutterudites.[58–60] In each of these systems, unstable cation coordination environments can lead to high anharmonicity and stronger phonon-phonon scattering. However, it is important to note that cage compounds such as clathrates differ from the layered system in the present study in that the clathrate cages are formed from stiff covalent anion-anion bonds that are not necessarily destabilized by undersized cations. In contrast, the anions in AMg_2Pn_2 compounds do not form bonds with anions in adjacent layers, meaning that small cations can potentially destabilize the entire structure, leading to highly anharmonic transverse acoustic phonons. In contrast, small or heavy fillers in cage compounds lead to flat, low-frequency optical modes that cross and interact with the stiff acoustic modes.[7]

Please cite this article in press as: Peng et al., An Unlikely Route to Low Lattice Thermal Conductivity: Small Atoms in a Simple Layered Structure, Joule (2018), https://doi.org/10.1016/j.joule.2018.06.014

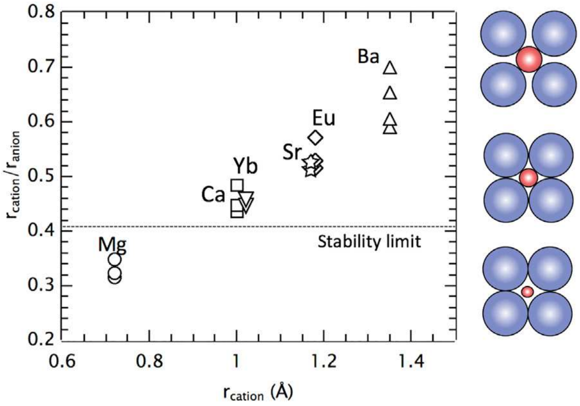

Figure 9. Cation:Anion Ratio Stability Limit

For octahedral coordination (CN = 6), Pauling's radius ratio rules predict a minimum stability limit of r_{cation}:r_{anion} = 0.414. For Ca, Sr, Eu, and Yb, this rule is satisfied. In contrast, the Mg cation is too small, which leads to a distorted octahedral environment and may be responsible for weak, anharmonic interlayer bonding.

Conclusion

Inherently low lattice thermal conductivity is typically associated with dense materials or compounds with complexity at the atomic scale or on a microstructural level. The unusually low lattice thermal conductivity of Mg_3Sb_2, in contrast, shows that structural instability alone is sufficient, even in a very simple structure, to cause exceptionally high phonon scattering rates and low lattice thermal conductivity. By combining *ab initio* phonon calculations and high-temperature elasticity measurements, we showed that Mg_3Sb_2 and Mg_3Bi_2 are highly anharmonic, in contrast to the Ca- and Yb-containing AMg_2Pn_2 compounds investigated here. Large mode Grüneisen parameters, both negative and positive, were predicted in the acoustic branches of Mg_3Sb_2 and Mg_3Bi_2 and are expected to have a large contribution to thermal transport. This was confirmed experimentally by the rapid decrease of the speed of sound and elastic moduli in Mg_3Sb_2 and Mg_3Bi_2 with increasing temperature, which is a direct consequence of the softening of the acoustic modes. We attribute this unique behavior to the small radii of Mg, which is undersized for the octahedrally coordinated cation site. The poor fit of the Mg cation is suspected to lead to weak interlayer bonding, and thus to the observed soft shear modes, and, ultimately, to the highly anharmonic behavior of the acoustic branches. These results suggest more broadly that soft shear modes resulting from undersized cations provide a potential path to low lattice thermal conductivity in ionic layered structures.

EXPERIMENTAL PROCEDURES

Synthesis

AMg_2Pn_2 compounds with A = Mg, Ca, Yb and Pn = Sb, Bi were synthesized by direct ball-milling of the elements followed by spark plasma sintering. The corresponding stoichiometric elements (99.8% Mg shot, 99.5% Ca shot, 99.9% Yb chunk, 99.99% Sb from Alfa Aesar, and 99.99% Rotometal Bi) were cut into small pieces in an argon-filled glovebox, loaded into stainless-steel vials with two 10-mm diameter stainless-steel balls, and milled for 1 hr using an SPEX mill. The powder was then loaded into graphite dies with 10-mm bores and sintered using the profile shown in Table 1 under a pressure of 31 MPa using a Dr. Sinter SPS-211LX. The pressure was removed immediately when cooling started. The densities of all the samples were obtained by measurement of mass and geometry. All samples were at least 97% of the theoretical

Please cite this article in press as: Peng et al., An Unlikely Route to Low Lattice Thermal Conductivity: Small Atoms in a Simple Layered Structure, Joule (2018), https://doi.org/10.1016/j.joule.2018.06.014

Table 1. Maximum Temperature and Hold Time Used during Spark Plasma Sintering of AMg_2Pn_2 (A = Mg, Ca, Yb and Pn = Sb, Bi) Samples

	Mg_3Sb_2	$CaMg_2Sb_2$	$YbMg_2Sb_2$	Mg_3Bi_2	$CaMg_2Bi_2$	$YbMg_2Bi_2$
Temperature (°C)	850	650	650	600	700	700
Time (min)	15	10	10	10	10	15

density. Phase purity was confirmed using a Rigaku X-ray diffraction system, showing that samples contained less than 3% of secondary phases.

Characterization

The temperature-dependent elastic moduli of all compositions were measured by resonant ultrasound spectroscopy (RUS)[39,40] using a custom modification of a Mangaflux-RUS Quasar 4000 system in a furnace with a flowing Ar atmosphere. Cylindrical samples were mounted on a tripod transducer setup. One transducer induced the mechanical vibrations and the remaining two detected the specimen resonances. The elastic moduli were measured in 20-K intervals from 303 K up to 673 K. The sinusoidal driving frequency was swept from 0 to 500 kHz. The RUS measurement at each temperature was typically completed within 1 min. Data were analyzed using commercial Quasar2000 CylModel software to match predicted and observed resonant frequencies.

Thermal expansion of all compositions was measured from 303 K to 573 K using a Rigaku Smartlab XRD instrument equipped with a high-temperature stage. The samples were ground into fine powders that were then placed on a graphite foil on top of a platinum tray. The measurements were performed under vacuum to prevent oxidation. The thermocouple inserts into the inner part of the platinum tray to increase the accuracy of the temperature measurement. The heating rate is 10 K/min with a 1-min hold, and sample height alignments were performed before each measurement to account for the combined thermal expansion of the holder and sample.

Calculation Details

The ABINIT software package[61–63] was used to perform density functional theory (DFT) and density functional perturbation theory simulations to obtain phonon properties and elastic constants.[64–67] The exchange-correlation energy was approximated using the PBEsol[68] functional, which has been proved to provide accurate phonon frequencies compared with experimental data.[69] Norm-conserving pseudopotentials[70] extracted from the PseudoDujo pseudopotentials table version 0.3[71] were used for all the elements. The Brillouin zone was sampled with 8 × 8 × 5 Monkhorst-Pack grids.[72–74] Due to the well-known underestimation of the band gap by standard DFT, we limit our analysis to Mg_3Sb_2, $CaMg_2Sb_2$ and $CaMg_2Bi_2$, which are correctly predicted to be insulating within the adopted approximations. The temperature-dependent thermodynamical properties were obtained in the framework of the quasiharmonic approximation from the phonon dispersion curves calculated at different fixed volumes V (while still relaxing the position of the atoms and the shape of the unit cell). Mode Grüneisen parameters were obtained as the logarithmic derivative of the phonon frequencies with respect to the volume:

$$\gamma_i = -\frac{V}{\omega_i}\frac{\delta\omega_i}{\delta V}, \qquad \text{(Equation 1)}$$

where V is volume and ω_i is the mode frequency. The averaged Grüneisen parameter γ has been calculated as the square root of the mode-averaged-squared Grüneisen parameter[75]

$$\gamma = \sqrt{\frac{\sum_{i,q}\gamma_{i,q}^2 C_{i,q}}{\sum_{i,q}C_{i,q}}}, \qquad \text{(Equation 2)}$$

Please cite this article in press as: Peng et al., An Unlikely Route to Low Lattice Thermal Conductivity: Small Atoms in a Simple Layered Structure, Joule (2018), https://doi.org/10.1016/j.joule.2018.06.014

where the summation is over all the modes and all the q points in the Brillouin zone. $C_{i,q}$ is the mode contribution to the heat capacity calculated at the Debye temperature θ_D,

$$\theta_D = n^{-1/3}\sqrt{\frac{5\hbar\int_0^\infty \omega^2 g(\omega)d\omega}{3k_b^2\int_0^\infty \omega^2 g(\omega)d\omega}}, \quad \text{(Equation 3)}$$

where n is the number of atoms per units cell and $g(\omega)$ is the phonon DOS.

SUPPLEMENTAL INFORMATION

Supplemental Information includes Supplemental Experimental Procedures, seven figures, three tables, and three videos and can be found with this article online at https://doi.org/10.1016/j.joule.2018.06.014.

ACKNOWLEDGMENTS

This work was supported by the NASA Science Missions Directorate's Radioisotope Power Systems Thermoelectric Technology Development Project. A.Z. additionally acknowledges support from the National Science Foundation, award number 1709158. G.H. acknowledges financial support from the FRS-FNRS through the PDR grants HiT4FiT (T.1031.14) and HTBaSE (T.1071.15). Computational resources were provided by the supercomputing facilities of the Université Catholique de Louvain (CISM/UCL) and the Consortium des Equipements de Calcul Intensif en Fédération Wallonie Bruxelles (CECI) funded by the Fonds de la Recherche Scientifique de Belgique (FRS-FNRS).

AUTHOR CONTRIBUTIONS

Conceptualization, A.Z. and G.H.; Investigation and Formal Analysis, W.P., G.P., A.Z., and G.H.; Resources, A.Z. and G.H.; Writing – Original Draft, W.P. and A.Z.; Writing – Review and Editing, W.P., G.P., G.H., A.Z., and G.-M.R.; Supervision, G.H., A.Z., and G.-M.R; Funding Acquisition, G.H., A.Z., and G.-M.R.

DECLARATION OF INTERESTS

The authors declare no competing interests.

Received: April 14, 2018
Revised: May 21, 2018
Accepted: June 15, 2018
Published: July 9, 2018

REFERENCES

1. Shi, L., Dames, C., Lukes, J.R., Reddy, P., Duda, J., Cahill, D.G., Lee, J., Marconnet, A., Goodson, K.E., Bahk, J.-H., et al. (2015). Evaluating broader impacts of nanoscale thermal transport research. Nanosc. Microsc. Therm. Eng. *19*, 127–165.
2. Biswas, K., He, J., Blum, I.D., Wu, C.-I., Hogan, T.P., Seidman, D.N., Dravid, V.P., and Kanatzidis, M.G. (2012). High-performance bulk thermoelectrics with all-scale hierarchical architectures. Nature *489*, 414.
3. Bux, S.K., Fleurial, J.-P., and Kaner, R.B. (2010). Nanostructured materials for thermoelectric applications. Chem. Commun. (Camb.) *46*, 8311–8324.
4. Klemens, P. (1955). The scattering of low-frequency lattice waves by static imperfections. Proc. Phys. Soc. *68*, 1113.
5. He, J., Kanatzidis, M.G., and Dravid, V.P. (2013). High performance bulk thermoelectrics via a panoscopic approach. Mater. Today *16*, 166–176.
6. Toberer, E.S., Cox, C.A., Brown, S.R., Ikeda, T., May, A.F., Kauzlarich, S.M., and Snyder, G.J. (2008). Traversing the metal-insulator transition in a Zintl phase: rational enhancement of thermoelectric efficiency in $Yb_{14}Mn_{1-x}Al_xSb_{11}$. Adv. Funct. Mater. *18*, 2795–2800.
7. Toberer, E.S., Zevalkink, A., and Snyder, G.J. (2011). Phonon engineering through crystal chemistry. J. Mater. Chem. *21*, 15843–15852.
8. Lee, S., Esfarjani, K., Luo, T., Zhou, J., Tian, Z., and Chen, G. (2014). Resonant bonding leads to low lattice thermal conductivity. Nat. Commun. *5*, 3525.
9. Madsen, G.K., and Santi, G. (2005). Anharmonic lattice dynamics in type-I clathrates from first-principles calculations. Phys. Rev. B *72*, 220301.
10. Lai, W., Wang, Y., Morelli, D.T., and Lu, X. (2015). From bonding asymmetry to anharmonic rattling in $Cu_{12}Sb_4S_{13}$

Please cite this article in press as: Peng et al., An Unlikely Route to Low Lattice Thermal Conductivity: Small Atoms in a Simple Layered Structure, Joule (2018), https://doi.org/10.1016/j.joule.2018.06.014

tetrahedrites: when lone-pair electrons are not so lonely. Adv. Funct. Mater. *25*, 3648–3657.

11. Skoug, E.J., and Morelli, D.T. (2011). Role of lone-pair electrons in producing minimum thermal conductivity in nitrogen-group chalcogenide compounds. Phys. Rev. Lett. *107*, 235901.
12. Lu, X., Morelli, D.T., Xia, Y., Zhou, F., Ozolins, V., Chi, H., Zhou, X., and Uher, C. (2013). High performance thermoelectricity in earth-abundant compounds based on natural mineral tetrahedrites. Adv. Energy Mater. *3*, 342–348.
13. Bansal, D., Hong, J., Li, C.W., May, A.F., Porter, W., Hu, M.Y., Abernathy, D.L., and Delaire, O. (2016). Phonon anharmonicity and negative thermal expansion in SnSe. Phys. Rev. B *94*, 054307.
14. Delaire, O., Ma, J., Marty, K., May, A.F., McGuire, M.A., Du, M.-H., Singh, D.J., Podlesnyak, A., Ehlers, G., Lumsden, M., and Sales, B.C. (2011). Giant anharmonic phonon scattering in PbTe. Nat. Mater. *10*, 614.
15. Bhardwaj, A., Rajput, A., Shukla, A., Pulikkotil, J., Srivastava, A., Dhar, A., Gupta, G., Auluck, S., Misra, D., and Budhani, R. (2013). Mg_3Sb_2-based Zintl compound: a non-toxic, inexpensive and abundant thermoelectric material for power generation. RSC Adv. *3*, 8504–8516.
16. Song, L., Zhang, J., and Iversen, B.B. (2017). Simultaneous improvement of power factor and thermal conductivity via Ag doping in p-type Mg_3Sb_2 thermoelectric materials. J. Mater. Chem. *5*, 4932–4939.
17. Shuai, J., Wang, Y., Kim, H.S., Liu, Z., Sun, J., Chen, S., Sui, J., and Ren, Z. (2015). Thermoelectric properties of Na-doped Zintl compound: $Mg_{3-x}Na_xSb_2$. Acta Mater. *93*, 187–193.
18. Shuai, J., Mao, J., Song, S., Zhang, Q., Chen, G., and Ren, Z. (2017). Recent progress and future challenges on thermoelectric Zintl materials. Mater. Today Phys. *1*, 74–95.
19. Peng, W., Chanakian, S., and Zevalkink, A. (2018). Crystal chemistry and thermoelectric transport of layered AM_2X_2 compounds. Inorg. Chem. Front. https://doi.org/10.1039/C7QI00813A.
20. Wood, M., Aydemir, U., Ohno, S., and Snyder, G.J. (2018). Observation of valence band crossing: the thermoelectric properties of $CaZn_2Sb_2$-$CaMg_2Sb_2$ solid solution. J. Mater. Chem. A *6*, 9437–9444.
21. Martinez-Ripoll, M., Haase, A., and Brauer, G. (1974). The crystal structure of α-Mg_3Sb_2. Acta Cryst. B *30*, 2006–2009.
22. De Jong, M., Chen, W., Angsten, T., Jain, A., Notestine, R., Gamst, A., Sluiter, M., Ande, C.K., Van Der Zwaag, S., Plata, J.J., et al. (2015). Charting the complete elastic properties of inorganic crystalline compounds. Sci. Data *2*, 150009.
23. Jain, A., Ong, S.P., Hautier, G., Chen, W., Richards, W.D., Dacek, S., Cholia, S., Gunter, D., Skinner, D., Ceder, G., and Persson, K.A. (2013). The Materials Project: A materials genome approach to accelerating materials innovation. APL Mater. *1*, 011002, https://doi.org/10.1063/1.4812323.
24. Tamaki, H., Sato, H.K., and Kanno, T. (2016). Isotropic conduction network and defect chemistry in $Mg_{3+\delta}Sb_2$-based layered zintl compounds with high thermoelectric performance. Adv. Mater. *28*, 10182–10187.
25. Zhang, J., Song, L., Mamakhel, A., Jørgensen, M.R.V., and Iversen, B.B. (2017). High-performance low-cost n-type Se-doped Mg_3Sb_2-based Zintl compounds for thermoelectric application. Chem. Mater. *29*, 5371–5383.
26. Zhang, J., Song, L., Pedersen, S.H., Yin, H., Hung, L.T., and Iversen, B.B. (2017). Discovery of high-performance low-cost n-type Mg_3Sb_2-based thermoelectric materials with multi-valley conduction bands. Nat. Commun. *8*, 13901.
27. Imasato, K., Kang, S.D., Ohno, S., and Snyder, G.J. (2017). Band engineering in Mg_3Sb_2 by alloying with Mg_3Bi_2 for enhanced thermoelectric performance. Mater. Horizons *5*, 59–64.
28. Shuai, J., Mao, J., Song, S., Zhu, Q., Sun, J., Wang, Y., He, R., Zhou, J., Chen, G., Singh, D.J., and Ren, Z. (2017). Tuning the carrier scattering mechanism to effectively improve the thermoelectric properties. Energ. Environ. Sci. *10*, 799–807.
29. Ohno, S., Imasato, K., Anand, S., Tamaki, H., Kang, S.D., Gorai, P., Sato, H.K., Toberer, E.S., Kanno, T., and Snyder, G.J. (2017). Phase boundary mapping to obtain n-type Mg_3Sb_2-based thermoelectrics. Joule *2*, 141–154.
30. Zhang, J., Song, L., Madsen, G.K., Fischer, K.F., Zhang, W., Shi, X., and Iversen, B.B. (2016). Designing high-performance layered thermoelectric materials through orbital engineering. Nat. Commun. *7*, 10892.
31. Shuai, J., Geng, H., Lan, Y., Zhu, Z., Wang, C., Liu, Z., Bao, J., Chu, C.-W., Sui, J., and Ren, Z. (2016). Higher thermoelectric performance of Zintl phases $(Eu_{0.5}Yb_{0.5})_{1-x}Ca_xMg_2Bi_2$ by band engineering and strain fluctuation. Proc. Natl. Acad. Sci. USA *113*, E4125–E4132.
32. Kuo, J.J., Kang, S.D., Imasato, K., Tamaki, H., Ohno, S., Kanno, T., and Snyder, G.J. (2018). Grain boundary dominated charge transport in Mg_3Sb_2-based compounds. Energ. Environ. Sci. *11*, 429–434.
33. Slack, G.A. (1979). The thermal conductivity of nonmetallic crystals. In Solid State Physics, *volume 34*, H. Ehrenreich, F. Seitz, and D. Turnbull, eds. (Elsevier), pp. 1–71.
34. Zeier, W.G. (2017). New tricks for optimizing thermoelectric materials. Curr. Opin. Green Sustain. Chem. *4*, 23–28.
35. Miller, S.A., Gorai, P., Ortiz, B.R., Goyal, A., Gao, D., Barnett, S.A., Mason, T.O., Snyder, G.J., Lv, Q., Stevanovic, V., and Toberer, E. (2017). Capturing anharmonicity in a lattice thermal conductivity model for high-throughput predictions. Chem. Mater. *29*, 2494–2501.
36. Singh, D.J., and Parker, D. (2013). Electronic and transport properties of zintl phase $AeMg_2Pn_2$, Ae= Ca, Sr, Ba, Pn= As, Sb, Bi in relation to Mg_3Sb_2. J. Appl. Phys. *114*, 143703.
37. Tani, J.-I., Takahashi, M., and Kido, H. (2010). Lattice dynamics and elastic properties of Mg_3As_2 and Mg_3Sb_2 compounds from first-principles calculations. Physica B Condens. Matter *405*, 4219–4225.
38. Tritt, T.M. (2005). Thermal Conductivity: Theory, Properties, and Applications (Springer Science & Business Media).
39. Li, G., and Gladden, J. (2010). High temperature resonant ultrasound spectroscopy: a review. Int. J. Spectrosc. https://doi.org/10.1155/2010/206362.
40. ASTM International. (2018). E1876-15: Standard test method for dynamic Young's modulus, shear modulus, and Poisson's ratio by impulse excitation of vibration. Annual Book of ASTM Standards *03.01*. https://www.astm.org/Standards/E1876.htm.
41. Jenkins, J., Rayne, J., and Ure, R., Jr. (1972). Elastic moduli and phonon properties of Bi_2Te_3. Phys. Rev. B *5*, 3171.
42. Grimsditch, M. (1983). Shear elastic modulus of graphite. J. Phys. C Solid State Phys *16*, L143.
43. Zabel, H. (2001). Phonons in layered compounds. J. Phys. Condens. Matter *13*, 7679.
44. Li, B., Wang, H., Kawakita, Y., Zhang, Q., Feygenson, M., Yu, H., Wu, D., Ohara, K., Kikuchi, T., Shibata, K., and Yamada, T. (2018). Liquid-like thermal conduction in intercalated layered crystalline solids. Nat. Mater. *17*, 226.
45. Li, G., Aydemir, U., Wood, M., An, Q., Goddard, W.A., III, Zhai, P., Zhang, Q., and Snyder, G.J. (2017). Deformation mechanisms in high-efficiency thermoelectric layered zintl compounds. J. Mater. Chem. A *5*, 9050–9059.
46. Ren, F., Case, E.D., Sootsman, J.R., Kanatzidis, M.G., Kong, H., Uher, C., Lara-Curzio, E., and Trejo, R.M. (2008). The high-temperature elastic moduli of polycrystalline PbTe measured by resonant ultrasound spectroscopy. Acta Mater. *56*, 5954–5963.
47. Schmidt, R.D., Case, E.D., Ni, J.E., Trejo, R.M., Lara-Curzio, E., Korkosz, R.J., and Kanatzidis, M.G. (2013). High-temperature elastic moduli of thermoelectric $SnTe_{1\pm x}$-y SiC nanoparticulate composites. J. Mater. Sci. *48*, 8244–8258.
48. Morelli, D.T., and Slack, G.A. (2006). High lattice thermal conductivity solids. In High Thermal Conductivity Materials, S.L. Shinde and J. Goela, eds. (Springer), pp. 37–68.
49. Ledbetter, H. (1994). Relationship between bulk-modulus temperature dependence and thermal expansivity. Phys. Status Solidi B *181*, 81–85.
50. Khatun, M., Stoyko, S.S., and Mar, A. (2013). Quaternary arsenides $AM_{1.5}Tt_{0.5}As_2$ (A= Na, K, Rb; M= Zn, Cd; Tt= Si, Ge, Sn): size effects in $CaAl_2Si_2$-and $ThCr_2Si_2$-type structures. Inorg. Chem. *52*, 3148–3158.
51. Klüfers, P., and Mewis, A. (1984). AB_2X_2-verbindungen mit $CaAl_2Si_2$-struktur. Z. Kristallog. Cryst. Mater. *169*, 135–148.
52. Pauling, L. (1960). The Nature of the Chemical Bond, *volume 260* (Cornell university press).
53. Giacovazzo, C., ed. (1992). Fundamentals of Crystallography (IUCr).

Please cite this article in press as: Peng et al., An Unlikely Route to Low Lattice Thermal Conductivity: Small Atoms in a Simple Layered Structure, Joule (2018), https://doi.org/10.1016/j.joule.2018.06.014

54. Shannon, R.T., and Prewitt, C.T. (1969). Effective ionic radii in oxides and fluorides. Acta Cryst. B *25*, 925–946.

55. Sevastâ yanova, L., Kravchenko, O., Gulish, O., Stupnikov, V., Leonova, M., and Zhizhin, M. (2006). Binary and ternary compounds in the Mg-Sb-B and Mg-Bi-B systems as catalysts for the synthesis of cubic BN. Inorg. Mater. *42*, 863–866.

56. Hong, J., and Delaire, O. (2016). Electronic instability and anharmonicity in SnSe. arXiv, 1604.07077.

57. Li, C.W., Hong, J., May, A.F., Bansal, D., Chi, S., Hong, T., Ehlers, G., and Delaire, O. (2015). Orbitally driven giant phonon anharmonicity in SnSe. Nat. Phys. *11*, 1063.

58. Nolas, G.S., Slack, G.A., and Schujman, S.B. (2001). Semiconductor clathrates: a phonon glass electron crystal material with potential for thermoelectric applications. In Semiconductors and Semimetals, *volume 69*, T. Tritt, ed. (Elsevier), pp. 255–300.

59. Nolas, G., Morelli, D., and Tritt, T.M. (1999). Skutterudites: a phonon-glass-electron crystal approach to advanced thermoelectric energy conversion applications,. Annu. Rev. Mater. Sci. *29*, 89–116.

60. Uher, C. (2001). Skutterudites: prospective novel thermoelectrics. In Semiconductors and Semimetals, *volume 69*, T. Tritt, ed. (Elsevier), pp. 139–253.

61. Gonze, X., Beuken, J.-M., Caracas, R., Detraux, F., Fuchs, M., Rignanese, G.-M., Sindic, L., Verstraete, M., Zerah, G., Jollet, F., et al. (2002). First-principles computation of material properties: the ABINIT software project. Comput. Mater. Sci. *25*, 478–492.

62. Gonze, X., Amadon, B., Anglade, P.-M., Beuken, J.-M., Bottin, F., Boulanger, P., Bruneval, F., Caliste, D., Caracas, R., Côté, M., and Deutsch, T. (2009). ABINIT: first-principles approach to material and nanosystem properties. Comput. Mater. Sci. *180*, 2582–2615.

63. Gonze, X., Jollet, F., Araujo, F.A., Adams, D., Amadon, B., Applencourt, T., Audouze, C., Beuken, J.-M., Bieder, J., Bokhanchuk, A., and Bousquet, E. (2016). Recent developments in the ABINIT software package. Comput. Phys. Comm. *205*, 106–131.

64. Baroni, S., de Gironcoli, S., Dal Corso, A., and Giannozzi, P. (2001). Phonons and related crystal properties from density-functional perturbation theory. Rev. Mod. Phys. *73*, 515–562.

65. Gonze, X. (1997). First-principles responses of solids to atomic displacements and homogeneous electric fields: implementation of a conjugate-gradient algorithm. Phys. Rev. B *55*, 10337–10354.

66. Gonze, X., and Lee, C. (1997). Dynamical matrices, born effective charges, dielectric permittivity tensors, and interatomic force constants from density-functional perturbation theory. Phys. Rev. B *55*, 10355–10368.

67. Hamann, D.R., Wu, X., Rabe, K.M., and Vanderbilt, D. (2005). Metric tensor formulation of strain in density-functional perturbation theory. Phys. Rev. B *71*, https://doi.org/10.1103/PhysRevB.71.035117.

68. Perdew, J.P., Ruzsinszky, A., Csonka, G.I., Vydrov, O.A., Scuseria, G.E., Constantin, L.A., Zhou, X., and Burke, K. (2008). Restoring the density-gradient expansion for exchange in solids and surfaces. Phys. Rev. Lett. *100*, 136406.

69. He, L., Liu, F., Hautier, G., Oliveira, M.J.T., Marques, M.A.L., Vila, F.D., Rehr, J.J., Rignanese, G.-M., and Zhou, A. (2014). Accuracy of generalized gradient approximation functionals for density-functional perturbation theory calculations. Phys. Rev. B *89*, 064305.

70. Hamann, D.R. (2013). Optimized norm-conserving vanderbilt pseudopotentials. Phys. Rev. B *88*, 085117.

71. van Setten, M., Giantomassi, M., Bousquet, E., Verstraete, M.J., Hamann, D.R., Gonze, X., and Rignanese, G.-M. (2018). The PseudoDojo: training and grading a 85 element optimized norm-conserving pseudopotential table. Comput. Phys. Comm. https://doi.org/10.1016/j.cpc.2018.01.012.

72. Monkhorst, H.J., and Pack, J.D. (1976). Special points for Brillouin-zone integrations. Phys. Rev. B *13*, 5188–5192.

73. Petretto, G., Gonze, X., Hautier, G., and Rignanese, G.-M. (2018). Convergence and pitfalls of density functional perturbation theory phonons calculations from a high-throughput perspective. Comput. Mater. Sci. *144*, 331–337.

74. Petretto, G., Dwaraknath, S., Miranda, H.P.C., Winston, D., Giantomassi, M., van Setten, M.J., Gonze, X., Persson, K.A., Hautier, G., and Rignanese, G.-M. (2018). High-throughput density functional perturbation theory phonons for inorganic materials. Sci. Data *5*, 180065.

75. Madsen, G.K.H., Katre, A., and Bera, C. (2015). Calculating the thermal conductivity of the silicon clathrates using the quasi-harmonic approximation. Phys. Status Solidi A *213*, 802–807.